Environ Monit Assess (2008) 137:111–126
DOI 10.1007/s10661-007-9733-z

Aerosol characteristics and surface radiative forcing components during a dust outbreak in Gwangju, Republic of Korea

K. O. Ogunjobi · Y. J. Kim

Received: 19 September 2006 / Accepted: 29 March 2007 / Published online: 26 April 2007

Abstract Atmospheric surface aerosol radiative forcing (SARF) ΔF, forcing efficiency ΔF_e and fractional forcing efficiency ΔFF_e evaluated from cloud-screened narrowband spectral and thermal-offset-corrected radiometric observations during the Asia dust outbreak episodes in Gwangju, Republic of Korea are reported in this study. Columnar aerosol optical properties (aerosol optical depth (AOD), $\tau_{a\lambda}$, Angstrom exponent α, mass concentration of fine and coarse mode particles) were also reported for the station between January 2000 and May 2001 consisting of 211cloud-free days. Results indicate that majority of the AOD were within the range 0.25–0.45 while some high aerosol events in which AODs≥0.6 were observed during the severe dust episodes. For example, AOD increases from annual average value of 0.34±0.13 at 501 nm to values >0.60 during the major dust events of March 27–30 and April 7–9, 2000, respectively. The $\alpha_{501-870\ nm}$ which is often used as a qualitative indicator of aerosol particle size had values ranging from 0.01 to 1.77. The diurnal forcing efficiency ΔDF_e at Gwangju was estimated to be -81.10 ± 5.14 W m^{-2}/$\tau_{501\ nm}$ and -47.09 ± 2.20 W m^{-2}/$\tau_{501\ nm}$ for the total solar broadband and visible band pass, respectively while the fractional diurnal forcing efficiency ΔFDF_e were $-15.8\pm0.64\%/\tau_{501\ nm}$ and $-22.87\pm1.13\%/\tau_{501\ nm}$ for the same band passes. Analyses of the 5-day air-mass back trajectories were further developed for Gwangju in order to classify the air-mass and types of aerosol reaching the site during the Asia dust episodes.

Keywords Radiative forcing · Forcing efficiency · Aerosols · Albedo · Asia dust · Air-mass trajectory

K. O. Ogunjobi · Y. J. Kim
Advanced Environmental Monitoring Research Center (ADEMRC), Gwangju Institute of Science and Technology, Gwangju 500-712, South Korea

K. O. Ogunjobi (✉)
Meteorologisches Institüt, Universität Bonn,
Auf dem Hügel str. 20,
53121 Bonn, Germany
e-mail: jobik2000@yahoo.com

Introduction

Aerosols in the atmosphere evolve in size and composition by homogenous and heterogeneous nucleation, condensation, coagulation as well as dry and wet deposition (Iziomon and Lohmann 2003). Aerosols have two major impacts in determining the radiative properties of the atmosphere as well as affecting its total energy budget. Firstly, the direct effects in which aerosol particles scatter and absorb solar and thermal radiation (Mitchell 1971; Coakley et al. 1983). The other is an indirect effect in which they change the particle size and lifetime of cloud droplets acting as cloud condensation nuclei, leading to cloud albedo

change (Twomey 1977; Rosenfeld and Lensky 1998). Moreover, the direct absorption of radiant energy by aerosols can influence the atmospheric temperature structure and, thus leading to cloud formation – a phenomenon often referred to as "semi-direct effect" (Ackerman et al. 2000; Koren et al. 2004). The addition of anthropogenic aerosols to the atmosphere may change the radiative fluxes at the top-of-atmosphere (TOA), at the surface, and within the atmospheric column. A positive radiative effect at the TOA indicates addition of energy to the earth-atmosphere system (i.e., a warming effect) whereas a negative effect indicates a net loss of energy (i.e., a cooling effect).

According to the Intergovermetal Panel on Climate Change IPCC (2001), radiative forcing of the surface-troposphere system in response to a perturbation is the change in net (downwelling minus upwelling) irradiance at the tropopause after allowing for stratospheric temperatures readjustment to radiative equilibrium, but with surface-tropospheric temperatures and state held fixed at the unperturbed values. There have been numerous efforts to estimate the surface aerosol radiative forcing. For example, Schafer et al. (2002) showed that, using sunphotometer retrieved aerosol optical depths, τ_a, with observed surface solar flux data, aerosol radiative forcing efficiencies due to smoke particulates during field campaign in Brazil and South Central Africa were determined to be −145 and −210 W/m^2/τ_a, respectively. Data from the Indian Ocean Experiment (INDOEX) have also been used to estimate the surface aerosol radiative forcing from anthropogenic haze in North Indian Ocean and Southeast Asia (Ramanathan et al. 2001; Bush et al. 2006). Christopher et al. (2003) used aerosol optical thickness retrievals from a geostationary satellite data (GOES 8 imager) as well as collocated surface fluxes measured by NASA's Surface Measurements for Atmospheric Radiative Transfer system (SWARF) to estimate top of atmosphere (TOA) radiative forcing and SARF during the Puerto Rico Dust Experiment (PRIDE). The monthly mean value and standard deviation of aerosol optical thickness at 670 nm during PRIDE were 0.26±0.13, and the corresponding monthly mean daytime SWARF values were −12.34±9.62 W m^{-2} at TOA and −18.13±15.81 W m^{-2} at the surface. Hansell et al. (2003) determined surface aerosol radiative forcing parameters using spectral and radiometric data obtained during PRIDE 2000, SAFARI 2000, and ACE-Asia 2001.

It is noted that the complex interaction of aerosols with radiation can further be investigated using three optical parameters namely, aerosol optical depth (AOD), single-scattering albedo (w_o), and the phase function (Yu et al. 2005). Aerosol optical thickness measures the magnitude of aerosol extinction (due to scattering and absorption) integrated in the vertical column. Single scattering albedo can be discussed as a parameter that characterizes absorption, because radiative transfer properties are sensitive to absorption via sensitivity to the ratio of scattering to total extinction rather than the absolute value of absorption. Therefore, the spectral dependence of w_o is driven by the spectral dependence of both absorption and scattering (Dubovik et al. 1998). In radiative transfer studies, w_o is defined as the ratio of scattering optical depth to the total optical depth (scattering + absorption) of the atmosphere which gives a measure of the effectiveness of scattering relative to extinction for light encountering the atmospheric aerosol particles (Dubovik et al. 2002). The wavelength-dependence of optical depth is usually represented by the Angstrom exponent α, with high values of α indicative of small particles and low values represent large particles.

This study focuses on the quantification of SARF using radiometric measurements taken at Gwangju Institute of Science and Technology during the period January 2000–May 2001. An attempt to provide such estimate at a new location Gwangju (Lat.35.13°N, Long.126.53°E) and during different Asia dust period in 2000 is herein presented. The atmospheric aerosols over the study area were generated from the Chinese/Mongolia desert, local biomass burnings, and industrial/urban sources. The scientific objectives of the study are as follows; Firstly, spectral measurements of solar flux from the multi-filter rotating shadow band radiometer (MFRSR-7) and surface fluxes from broadband radiometer are processed during the experimental campaign. The time series of AOD (τ_a), Angstrom exponent and particle mass concentration were investigated for selected dates during the periods under consideration. Secondly, by use of solar irradiance measurements from collocated visible radiometer (400–700 nm) along with the time series of retrieved AOD, quantitative estimates of the SARF are computed during the Asia dust spells of 2000 and 2001. The aerosol radiative

forcing, which is a measure of the aerosol radiative effects and the forcing efficiency, defined as the derivative of surface flux with respect to the aerosol optical depth were further investigated.

Study site and instrumentation

Gwangju, (Lat.35.13°N, Long.126.53°E) is a metropolitan city surrounded by high mountains with an altitude of 50 m above sea level. The city is characterized by high population density with limited industries but predominant agricultural activities and high fossil fuel combustion. Synoptically , the year can be subdivided into four seasons: (1) winter (December–February) usually very cool and dry; (2) spring (March–May), which is characterized by the transfer of aerosols with downstream wind from North East China and the inner Mongolia desert region (3) Summer (June–August), high and transparent cloud prevail with high solar irradiance while some days are wet with varying forms and intensity of cloudiness; (4) autumn (September–November), often associated with moderately transparent skies with morning mist, high relative humidity and high biomass burning.

The primary instrumentation used in this study includes the MFRSR-7 and the Total Solar Pyranometer (TSP) from Yankee Environmental Systems (YES). The MFRSR contains narrowband visible and near-infrared interference filters, each 10-nm full width half-maximum (FWHM). The MFRSR channels consist of seven different wavelengths band pass at 401, 501, 616, 675 870 and 940 nm in addition, it contains one unfiltered broadband silicon pyranometer whose spectral response is 200–4,000 nm. The MFRSR uses an automated rotating shadow band to make measurements of the global and diffuse components of solar irradiance. Once these two components are known, a central processing unit (CPU) can readily compute the direct-normal components. MFRSR-7 calibration, performed every 6 months at the YES laboratory, involves evaluating the angular, spectral, and absolute responses for each channel. Instrument output is subject to uncertainty owing to variations in the ambient temperature, which has been shown to be in the range of 1–2% per 1-K change in sensor-head temperature (Hansell et al. 2003). The measured uncertainty in the estimated AOD is estimated to be 0.01–0.02. The limiting accuracy for this instrument is ±0.3° because of stepping precession and a cosine error that is better than 5% for 0–80° zenith angle but better than 1% with corrections.

Methodology

Cloud-screening procedure

In order to reduce the uncertainties in retrieved aerosol optical depths from cloudy data sets, different statistical cloud-screening techniques have been developed (Conant 2000). The cloud-screening technique adopted in this study is herein explained. For the same solar zenith angle, the direct component of the surface downward solar irradiance is generally larger for a clear day than that of a cloudy atmosphere. However, the diffuse component is usually smaller for the clear atmosphere than for a cloudy atmosphere owing to additional scattering by cloud particles. Thus, the surface diffuse flux in conjunction with the direct solar flux is used to develop the cloud-screening scheme. A parameter defined as the ratio of the observed diffuse flux to the observed direct flux, normalized by air mass and total solar irradiance called the scatter ratio is developed. This parameter is a measure of the scattering effects of clouds. First, the analysis intervals (either morning or afternoon) for each regression are selected by air-mass range from 1.75 to 6. Lower air -masses are not used (even if available in the data) because the rate of change of the air mass is relatively small, creating a greater opportunity for changing atmospheric conditions that affect the regression. Higher air masses are avoided because of the greater uncertainty in air mass caused by refraction corrections that are increasingly sensitive to atmospheric temperature profiles. A forward finite-difference derivative filter then identifies regions where the slope of dI (λ)/d (Airmass) is positive which cannot be produced by any uniform airmass turbidity process, and is evidence of the recovery of the direct-normal irradiance from a cloud passage. Data points associated with solar zenith angles greater than 80° were automatically discarded. The cloud screening process then takes successive averages of the scatter ratios. A conventional least-squares regression is then performed on the remaining

points. During each iteration data points greater than the average plus one standard deviation are discarded. The points that remain are then used for a final least-squares regression that yields the final analysis product.

Determination of aerosol optical depth

Optical depth τ_λ can be derived from the Beer–Bouguer-Lambert's law in the form (Dutton et al. 1994)

$$I(\lambda) = E_o I_o(\lambda) e^{-m\tau(\lambda)} \quad (1)$$

where $I(\lambda)$ is the measured instrument voltage , E_o is a correction factor for the variations in the Sun–Earth distance, m is the refractive path length through the atmosphere when the measurement is made, $\tau(\lambda)$ is the optical depth for each wavelength λ and $I_o(\lambda)$ is the extraterrestrial flux in unit of volts. From Eq. 1, spectral total optical depth, represented as the sum of atmospheric constituents can be expressed as follows:

$$\tau(\lambda)m = \sum \tau_i(\lambda)m_i \quad (2)$$

In order to obtain the AOD from Eq. 2, it is necessary to consider the wavelength-dependent attenuation of solar radiation by minor constituents of the atmosphere denoted as symbol i. Once the total optical depths have been determined ,the corresponding values of the spectral aerosol optical depth, ($\tau_{a\lambda}$) were determined by subtracting from the total optical depth, (τ_t) contributions due to molecular scattering τ_R known as the Rayleigh optical depth, and the contribution of the ozone Chappuis absorption band τ_{O3} known as the ozone optical depth. Further corrections to the total optical depth were made for bands of strong selective absorption by atmospheric gases, however, since this study does not investigate bands for water vapor absorption, the optical depth due to water vapor was neglected.

Aerosol Angstrom exponent

In order to examine the aerosol size distribution from the MFRSR-7 solar irradiance data at Gwangju, the Angstrom empirical turbidity relation (Angstrom 1964; King et al. 1999) was employed:

$$\tau(\lambda) = \beta\lambda^{-\alpha} \quad (3)$$

where α and β are the Angstrom exponent (or shaping factor) and the turbidity coefficient, respectively. AOD and β are essentially synonymous quantities relating to λ, both being logarithmic indices of the atmospheric optical attenuation to a vertical beam (Jacovides et al. 2005). The components α and β can be computed by performing a linear regression fit on the plot of the logarithm of τ_a against logarithm of λ. However, in this study, we adopted an alternative method in evaluating the shaping factor α. The shaping factor is approximated by taking the logarithm of the ratio of the Angstrom's Power law expression at two λ (for this study λ=501 and 870 nm);

$$\delta = \tau_\alpha(\lambda_1)/\tau_\alpha(\lambda_2) = (\lambda_2/\lambda_1)^{(-\alpha)} = \gamma^{(-\alpha)} \quad (4)$$

Therefore, the Angstrom exponent can be determined from

$$\alpha = -\ln(\tau_{\alpha\lambda 1}/\tau_{\alpha\lambda 2})/\ln(\lambda_2/\lambda_1) \quad (5)$$

The shaping factor α characterizes the spectral features of the aerosol and it also relates to the size of the particles. Larger particles generally correspond to smaller α and vice versa.

Aerosol surface radiative forcing and forcing efficiency

Atmospheric forcing is a commonly used parameter in quantifying the effect of aerosols on the atmospheric energy budget usually expressed as diurnal average or instantaneous radiative forcing ΔF. This study is focused mainly on the radiative forcing in the broadband solar irradiance band pass and the visible band pass. Atmospheric radiative forcing defined as the difference between the net flux at the surface and the same quantity when there is no-aerosol present in the atmosphere can be expressed as (Bush and Valero 2002, 2003):

$$\Delta F = F_N - F_N^o \quad (6)$$

where the net flux F_{net} is the difference between the downwelling flux, F_{DW} and upwelling flux, F_{UP}. Since the upwelling flux is not measured directly for

this study, it was estimated in term of the downwelling and the broadband surface albedo A_b computed to be 0.085.

$$F_{UP} = A_b \times F_{DW} \quad (7)$$

The resulting surface radiative forcing then becomes

$$\Delta F = (1 - A_b) \times \left(F_{DW} - F_N^o\right) \quad (8)$$

The downwelling surface fluxes used as a reference in determining the atmospheric forcing during this period is estimated by the MODTRAN 4.0 atmospheric model (Anderson et al. 1999; Beck et al. 1999) free of aerosols and cloud. The meteorological profile measurement is taken from in situ balloon sounding provided by the Korea Meteorological Administration (KMA). The model calculation represents the basis for estimating the cloud and aerosol free environment. The result of the non-aerosol runs for a less polluted day on 5 April 2000 and severe Asian dust episode of 7 April 2000 is shown in Fig. 1a and b, respectively. Observation indicates that the computed average daily AOD is higher on 7 April than the value obtained for 5 April 2000 as discussed fully in "Aerosol optical depth and Ångström parameter." It should be noted that for the essentially cloud-free cases (with cloud amount <0.3/10) on 5 April and 7 April 2000, the difference between the no-aerosol runs (pristine case) and the measured solar irradiance gives the effect of the aerosols present in the atmosphere. The decrease in aerosol on 5 April relative to 7 April 2000 is indicated by the smaller difference between the flux measurements and the aerosol free atmosphere model runs.

Results and discussion

Aerosol optical depth and Ångström parameter

Daily measurements of the aerosol optical depth (AOD) at 501 nm were computed at every minute from the solar zenith angle of 76° in the morning to 76° in the evening. The data are then averaged as daily measurements from January 2000 to May 2001 consisting of 211 cloud-free days as shown in Fig. 2a. Also indicated in Fig. 2a are the severe dust spell days for 2000 and 2001, respectively. Large day–day variation in the daily average values of $\tau_{a501\ nm}$ is clearly displayed. A distinct annual pattern with an increase to peak AOD values in the spring period (March–May) is observed for the 2 years. For example, AOD increases from annual average value of 0.34±0.13 at 501 nm to values >0.60 during the major dust event days of March 27–30 and April 7–9, 2000. Computed daily maximum values of AOD similarly yield high AOD values of 0.71, 0.60 and 0.56 during the Asian dust storm episodes of 13, 24–25 April 2001, respectively. Ogunjobi et al. (2003) reported high aerosol conditions with corresponding high diffuse radiation on 12 April 2001 persisting through to the next day 13 April. After the intense dust storm of 13 April there is a drastic reduction in the diffuse irradiance persisting through to 18 April from ~0.34 to ~0.25 W/ (m^2nm), with a corresponding increase in the total and direct irradiance. This explains the strong response of solar radiation to varying atmospheric aerosol loading at the study site. Also interesting to note are periods with biomass burning at the study site in October of each year and occasionally in June (Ogunjobi et al. 2004). Higher AOD values recorded at Gwangju during this period is in agreement with the findings of Bush and Valero (2003) for Gosan, Republic of Korea during the ACE Asia dust storm of 13 April 2001. For comparison, higher AOD values ($\tau_{a500\ nm}$>3.0) were also recorded for Ilorin, Nigeria during the "harmattan" dust haze of 30 January 2000 (Pinker et al. 2001). The derived daily Angstrom exponent α for λ=501 and 870 nm is shown in Fig. 2b for the whole period of measurements. The Angstrom exponent provides a measure of how rapidly AOD is changing with wavelength and it also related to the size of the particles (Hansell et al. 2003; Dubovik et al. 2002). Figure 2b clearly illustrates the inverse dependence of the AOD and α with α varying between 0.01 in April (dust spell period) and 1.77 in August (dust free period). For example as AOD increased from a mean of 0.34±0.13 to 0.71 and 0.56 on 7 April 2000, and 25 April 2001, respectively, a drop in α value is observed from 1.05 on 6 April to 0.37 on 7 April 2000, and also from 0.87 on 15 April to 0.24 on 25 April 2001 (see Table 1). This relationship compares well with result of desert dust aerosols at Bahrain and Dalanzadgad, Mongolia reported by Eck et al. (1999). Other studies that

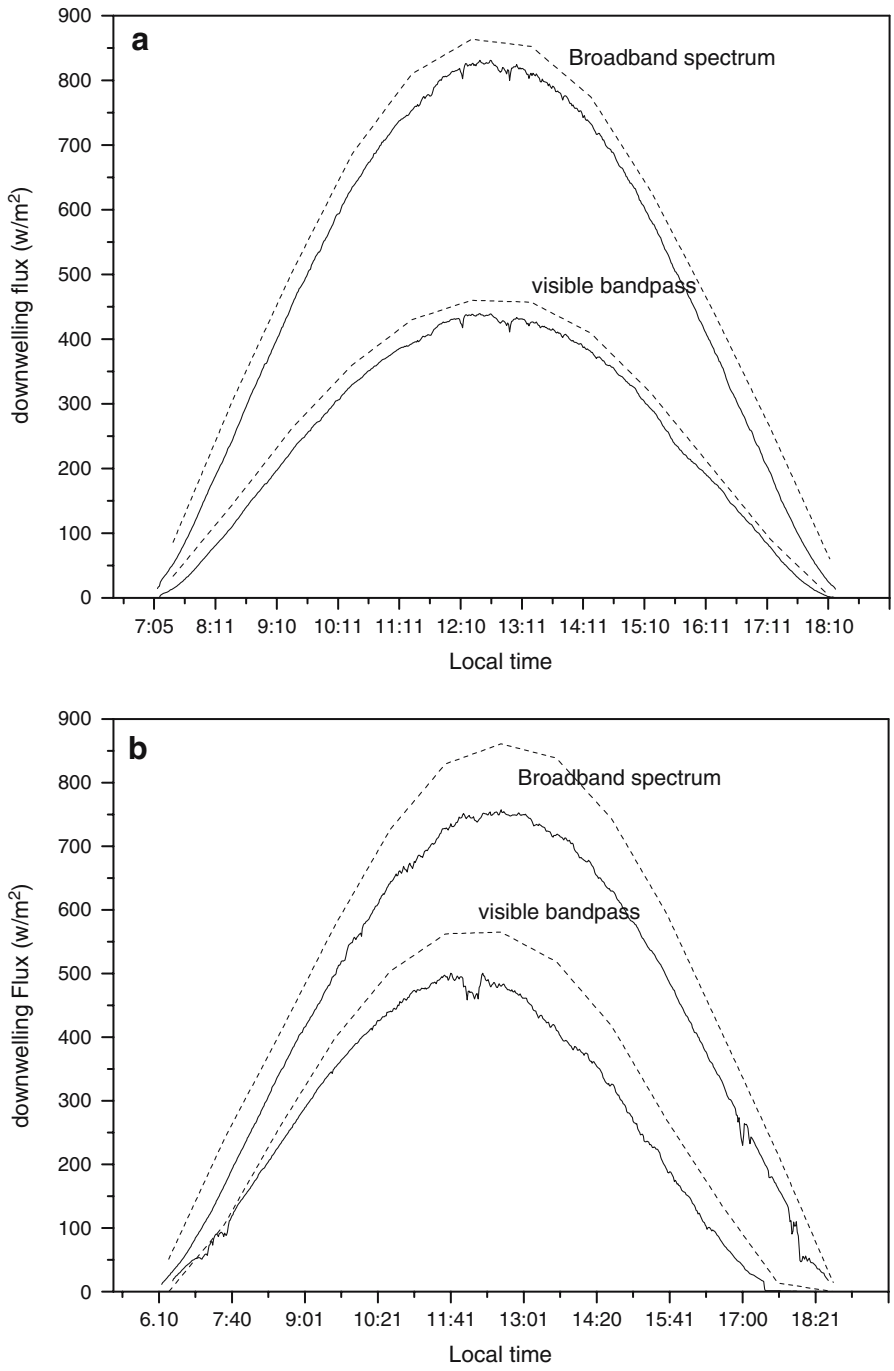

Fig. 1 Broadband and visible fluxes at Gwangju measured on **a** 5 April and **b** 7 April 2000 with the addition of aerosol-free model calculations (*dash lines*). All solar irradiance measurements were made at every 1-s under cloud-free atmospheric condition, with at least 760 observations made for each plot

reported similar trends include Pinker et al. (2001), Holben et al. (2001), Dubovik et al. (2002), Kim et al. (2004), and Eck et al. (2005).

Scatter plot of daily mean AOD at 501 nm versus α is given in Fig. 3a. Mean AODs for the four α ranges (0–0.5, 0.5–1.0, 1.0–1.5, and 1.5–2.0) are given in circles with the error bars indicating the respective standard deviation. Gwangju shows large α variation while AODs are mostly between 0.08 and 0.6 except for cases of Asia dust episodes. The

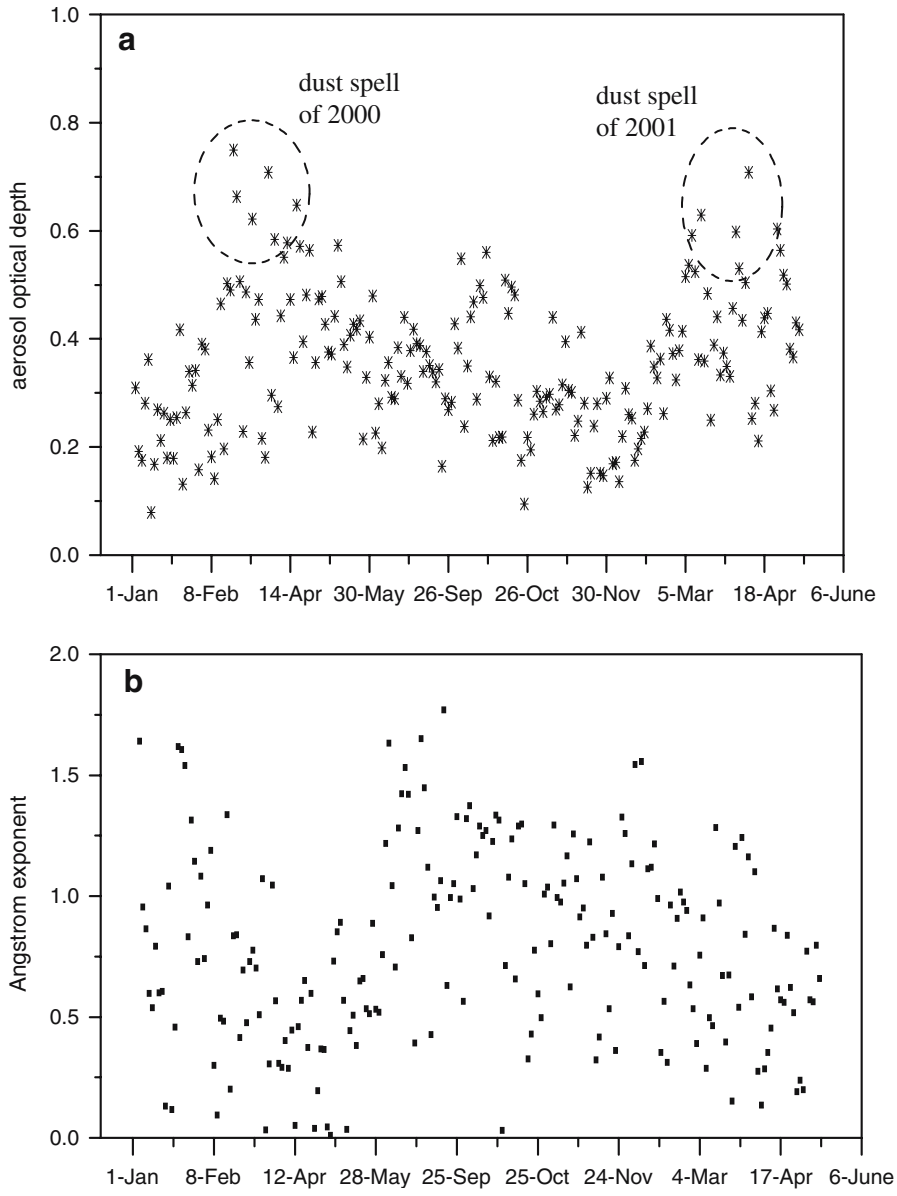

Fig. 2 **a** Daily average values of AOD (501 nm) at Gwangju, Republic of Korea for the cloud free days during the measurement period of January 2000–May 2001. **b** Daily average Angstrom exponents ($\alpha_{501-870\ nm}$) for the same data as shown in Fig. 2a

scatterplots may be separated into two dominant patterns. Firstly, an increasing α with increasing AOD which suggest fine particles dominance under the influence of biomass burning /local anthropogenic pollution at Gwangju during the measurement period. Secondly, the decreasing of α (<0.5) with increasing of AOD which is typical of the spring-time transport of high Asia dust observations to Gwangju resulting from a strong influence of coarse mode desert dust aerosol (Eck et al. 2005). A histogram of AOD over all the clear sky conditions (211 days) at Gwangju is shown in Fig. 3b. The majority of the AOD is within the range 0.25–0.45. It is clearly seen that there were also some relative clean cases where AODs are less than 0.1 and some high aerosol events especially during the Asian dust days in which AODs were over 0.6.

Table 1 illustrates further the characteristics of the aerosol type and corresponding mass concentration of fine and coarse particles as well as the PM_{10} measure-

Table 1 Characteristics of aerosol type, NCEP 5 days back trajectory and mass concentration of fine and coarse particles during episodes of dust, urban pollution, and biomass burning at Gwangju, Korea

Date	τ_α (λ= 510 nm)	α(501-870 nm)	Fine ($\mu g/m^3$)	Coarse ($\mu g/m^3$)	PM_{10} ($\mu g/m^3$)	Aerosol type	Airmass pathway
30 Mar 00	0.23	0.73	18.61	48.29	69.71	Mixed	Western China
7 Apr 00	0.71	0.37	29.01	86.03	109.75	Asian dust	Taklamakan/ Gobi Desert
15 Apr 00	0.47	0.46	11.48	42.97	39.41	Mixed	Western China
11 Apr 01	0.43	0.13	50.00	154.00	204.00	Asian dust	Taklamakan/ Gobi Desert (NW/W China)
12 Apr 01	0.50	0.29	20.90	39.90	60.80	Mixed	Western/central China
13 Apr 01	0.71	0.35	31.60	60.90	98.90	Asian dust	Taklamakan/ Gobi Desert (NW/W China)
19 Apr 01	0.44	0.56	30.30	45.40	75.70	Mixed	Eastern China
22 Apr 01	0.30	0.96	21.50	30.70	52.20	Pollution	North Korea
25 Apr 01	0.56	0.24	45.40	82.20	127.60	Asian dust	Eastern China across to Korea
10 May 01	0.52	0.53	14.90	13.90	31.71	Mixed	Eastern China across to Korea
12 May 01	0.38	1.37	13.80	6.20	33.0	Pollution	Eastern China across to Korea
9 June 01	0.46	1.16	65.70	5.40	105.33	Biomass	Western China/local pollution

ments in $\mu g/m^3$ during episodes of dust, urban pollution and biomass burning at Gwangju according to different air masses classification. Airmass back trajectories developed from Meteorological data provided by the National Center for Environmental Prediction (NCEP) were used for the air mass classifications. The detail description of the routine aerosol monitoring methods can be found in Ogunjobi et al. (2004); Kim et al. (2001). However a brief description is herein made. An air pollutant sampler URG-VAPS (model 2000J) with three filter packs and a Wide Inlet Sequential air sampler (WINS, R&P Partisol-Plus Model 2025) with one filter pack were used for the aerosol sample for both the fine particles with aerodynamic diameter $\leq$ 2.5 μm, and coarse particles with aerodynamic diameter up to 10 μm. Back trajectory analysis of the air masses in the atmospheric column over Gwangju indicate that the region was influenced by a number of different source regions throughout the dust periods and thus a wide variety of aerosol types (Merrill 2001; Ogunjobi et al. 2004). For example, in all of the dust cases, the air arriving at Gwangju originates from Gobi (40°~45°N, 90°~110°E) or Taklamakan desert (35°~40°N, 80°~90°E) in all the identified layers (200, 500 and 1,000 m). Due to the location of these desert sources, they are the major dust source regions in East Asia region. The lofted dust aerosols are transported eastward, affecting Japan and Korea. The pollution aerosols are always associated with at least one of the layers from Western China and on the average associated with higher precipitable water vapor in this region.

Average diurnal radiative forcing (ΔDF)

Result from surface measurement at Gwangju for which a greater part of the day is cloud free, the diurnal averaged radiative forcing was estimated as the integrated radiative forcing ΔF at the surface averaged over a 24-h period in the broadband (200–4,000 nm) and visible band pass (400–700 nm). For the sampled severe dust spell days of 7 April 2000 and 25 April 2001, the diurnal average forcing was estimated to be $\Delta DF = -58.4$ and -48.2 W m^{-2} for the broadband solar irradiance band pass, respectively. In the visible band pass, the ΔDF were −36.6 and −28.6 W m^{-2}, respectively. It is important to further

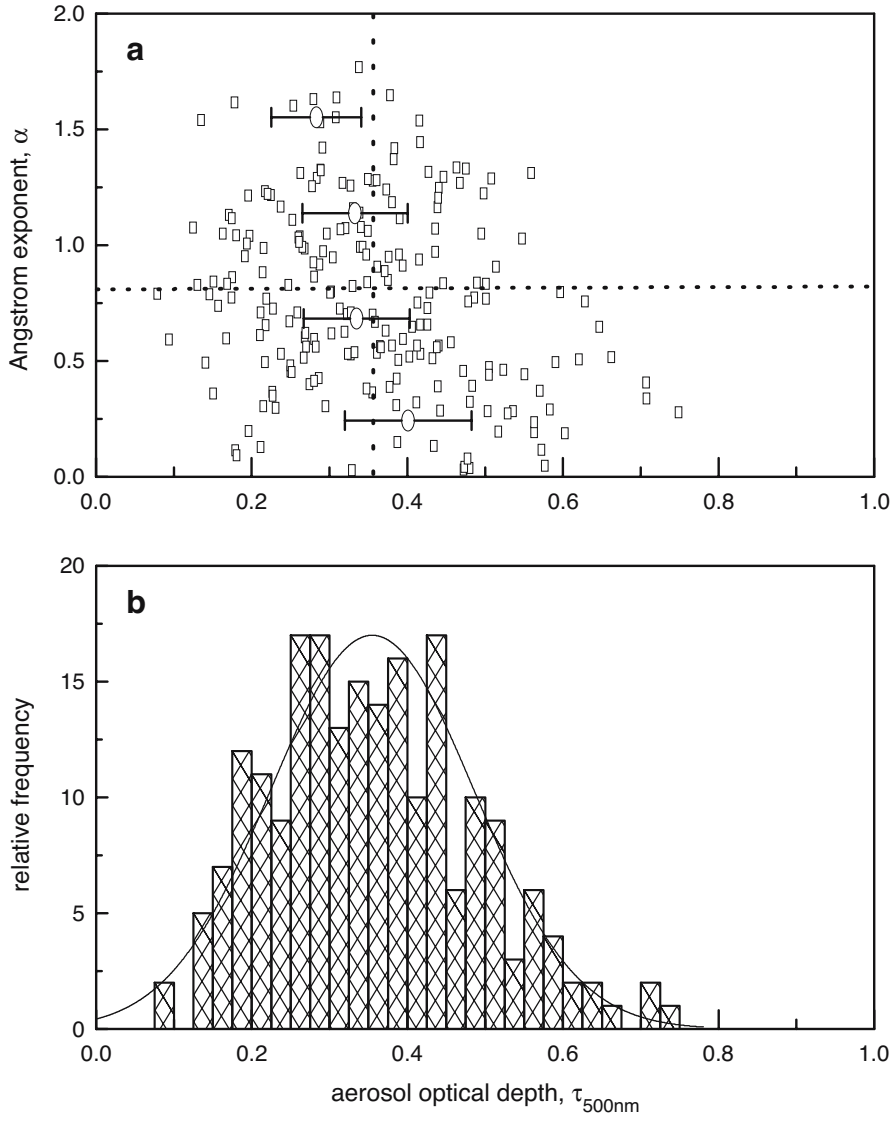

Fig. 3 **a** Scatterplots of the daily averaged AOD (501 nm) and Angstrom exponent. The *dotted lines* are the means values of α – AOD. Open circles and the error bars indicates AOD averages and the standard deviations given at four alpha ranges. **b** Illustrates the histogram of the AOD at Gwangju during the measurement periods January 2000–May 2001

explain the relationship between the magnitudes of the diurnal forcing and the average AOD during the periods under investigation. The average aerosol optical depths were 0.71 and 0.56 on 7 April and 25 April 2001, respectively (Table 2). The diurnal average forcing values at Gwangju compare well with the radiative forcing of −52.1 W m^{-2} computed by Bush and Valero (2003) on 13 April 2001 at Gosan with corresponding average τ_{a500nm} of 0.708± 0.038. Model estimates by Xu et al. (2003) also indicates that the mean cloud-free 24-h average radiative forcing at Linan in Yangtze delta region of China from 28 October to 1 December , 1999 was −28.6 W m^{-2} for total solar radiation (0.2–4.0 μm) and −16.0 W m^{-2} for the photosynthetically active radiation band (0.4–0.7 μm).

In order to understand the aerosol forcing efficiency trends, it is instructive to have a range of high and low aerosol optical depths as low aerosol conditions are presumed to be most useful in validating the components used in calculating the radiative forcing. A summary of the diurnal average forcing values for 11 clear days during 2000 and 2001 at Gwangju were computed and shown in Table 2 for the broadband

Table 2 Average daily AOD and diurnal radiative forcing for clear days (cloud amount <3/10) at Gwangju during spring time Asian dust episode

	Average AOD	Angstrom exponent $\alpha_{\alpha(501 \text{ and } 870 \text{ nm})}$	Radiative forcing (BB)W/m^2	Radiative forcing (Vis)W/m^2
30-Mar-00 (AM,PM)^{As}	0.23	0.73	−15.8±1.8	−10.4±1.2
1-Apr-00 (AM)	0.36	0.70	−22.7±1.6	−14.5±1.4
5-Apr-00 (AM)	0.22	0.31	−12.6±1.3	−9.2±0.5
6-Apr-00 (AM,PM)	0.16	1.05	−10.8±0.8	−7.2±0.2
7-Apr-00 (Am, PM)^{As}	0.71	0.37	−58.4±4.7	−36.6±2.5
8-Apr-00 (PM)	0.30	0.31	−31.2±2.2	−18.5±1.2
10-Apr-00 (AM,PM)	0.27	0.40	−19.7±1.9	−12.5±1.2
12-Apr-01 (AM,PM)^{As}	0.50	0.29	−40.8±3.2	−20.1±1.8
15-Apr-01 (AM,PM)	0.28	0.87	−18.4±2.1	−11.6±1.2
23-Apr-01 (AM,PM)	0.27	0.52	−16.9±1.8	−7.9±0.7
25-Apr-01 (AM,PM)^{As}	0.56	0.24	−48.2±3.8	−28.6±2.2

BB Broadband solar spectrum (200–4000 nm)

Vis Visible band pass (400–700 nm)

As indicates reported Asia dust storm days

spectrum and the visible band pass. Also indicated are the average daily AOD, the Angstrom exponent, during the dust episode of 2000 and 2001. It is observed that though the aerosol composition and magnitude may vary during the periods of measurement, the ratio between ΔDF and daily average AOD indicates the effectiveness of atmospheric perturbing by aerosols (i.e. the larger the ratio, the greater the forcing per unit optical depth). The frequent Asia dust aerosol outbreak is reflected in the variation of the radiative forcing during the period of analysis. Result from Table 2 also illustrates that the dust aerosols have larger influence on the energy budget as reflected from the magnitude of radiative forcing during the severe Asia dust outbreak days than other days at the site. The study also confirms the existence of a cooling effect (negative forcing) due to the direct effects of aerosols at the surface during the dust outbreak seasons. The estimated average top of atmosphere (TOA) fluxes were 497.9 and 507.7 W m^{-2} for the broadband total solar irradiance indicating that the fractional diurnal forcing ÄFDF values were −11.7 and −9.5% for the severe dust episode days of 7 April 2000 and 25 April 2001, respectively. Similarly, in the visible region, the top of atmosphere fluxes were 203.1 and 214.8 W m^{-2} which gives ΔFDF values of −18.0 and −13.3% at Gwangju for 7 April 2000 and 25 April 2001, respectively.

Forcing efficiency (ΔF_{eff})

The absolute magnitude of the surface radiative forcing in a location is explicitly determined by the quantity, type of aerosols perturbing the environment together with the amount of radiant energy entering the atmosphere (Bush and Valero 2003). The rate at which the atmosphere is forced per unit AOD is called the forcing efficiency. Figure 4 shows ΔF plotted against the aerosol optical depth for the entire Asian dust period of 2000 and 2001 at Gwangju. The slope of the linear fit of the radiative forcing in Fig. 4 yields the forcing efficiency ΔF_e which corresponds to the aerosol present in a localized region, defined as the rate at which the atmosphere is forced per unit optical depth. For the broadband and visible band passes, the forcing efficiencies at Gwangju were computed as −180.84± 6.68 W m^{-2} and −98.92±4.29 W m^{-2} per unit optical depth, respectively. The scatter plot shows a definite dependence of both broadband and visible radiative forcing on the magnitude of the aerosol optical depth and varying aerosol characteristics during the mea-

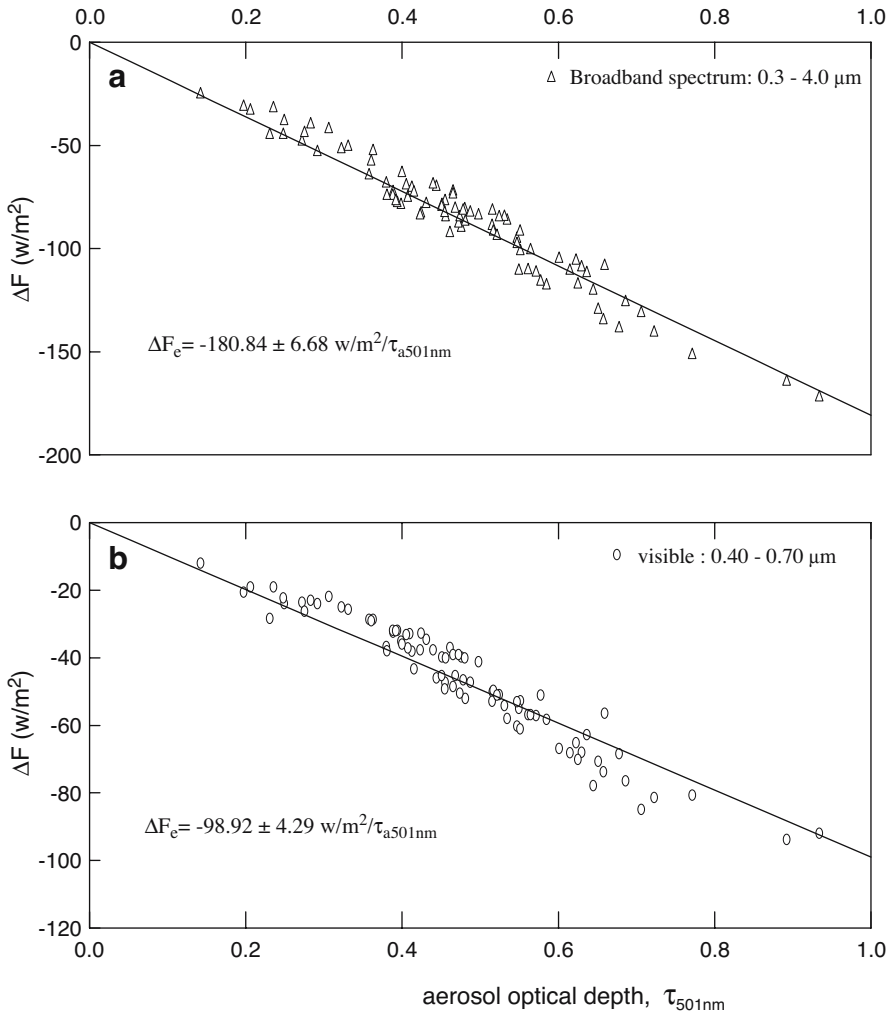

Fig. 4 The broadband and visible spectrum radiative forcing as a function of the AOD (λ=501 nm) for all cloud free atmosphere at Gwangju during Asia dust episodes of 2000 and 2001

surement periods. Performing similar analysis to ΔDF and ΔFDF in terms of the estimated AOD at Gwangju gives values of the diurnal forcing efficiency ΔDF_e and the fractional diurnal forcing efficiency ΔFDF_e as illustrated in Figs. 5 and 6, respectively. Estimated ΔDF_e were -81.10 ± 5.14 W $m^{-2}/\tau_{501\ nm}$ and -47.09 ± 2.20 W $m^{-2}/\tau_{501\ nm}$ for the broadband and visible band pass, respectively. The fractional diurnal forcing efficiency ΔFDF_e for the broadband and visible band pass were $-15.8 \pm 0.64\%/\tau_{501\ nm}$ and $-22.87 \pm 1.13\%/\tau_{501\ nm}$, respectively. It is important to note here that though the absolute ΔDF_e in the broadband is greater than the visible spectrum, the ΔFDF_e is however greater for the visible spectrum. This explains that the aerosols in the earth's atmosphere have much greater effect in perturbing the visible portion of the solar spectrum than the entire broadband. The Independent measurements of ΔDF_e at the Kaashidhoo Climate observatory (KCO) during the INDOEX experiment computed ΔDF_e values of -70 to -75 W $m^{-2}/\tau_{a\ddot{e}}$ for the total solar spectrum and ~ -38 to -40 W $m^{-2}/\tau_{a\ddot{e}}$ for the visible band pass (Satheesh and Ramanathan 2000; Bush and Valero 2002). Similarly, at Gosan, South Korea, during the ACE-Asia campaign Bush and Valero (2003) reported ΔDF_e values in the range of -73.0 and -42.2 W m^{-2}/

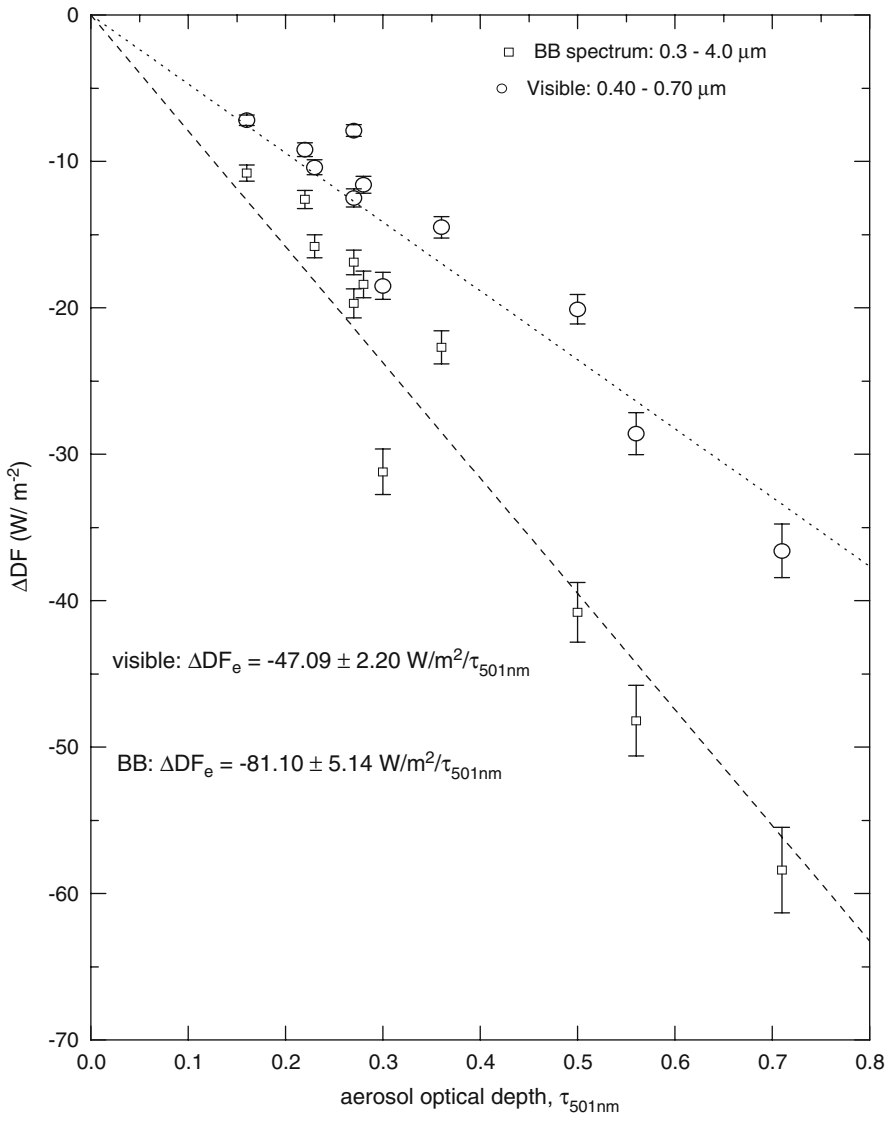

Fig. 5 Broadband and visible band passes diurnal forcing plotted against the average daily AOD (λ= 501 nm) for the selected clear days which cloud amount is <3/10 during the Asia dust episodes of 2000 and 2001. The uncertainty in the diurnal radiative forcing is indicated as *error bars*

$\tau_{a\ddot{e}}$ for same spectral regions. The magnitude of these forcing efficiencies are smaller (about 10 %) but still comparable to those found in this study during dust storm periods of 2000 and 2001 (i.e. −81.10 and 47.09 W m^{-2}/$\tau_{a\ddot{e}}$ for the broadband and visible band pass). Won et al. (2004) reported a forcing efficiency of −76.8±10.4 W m^{-2}/τ_{a500nm} at the surface for spring 2001 for the same site while Yoon et al.(2005) estimated a forcing efficiency of −101.9±17.2 W m^{-2}/$\tau_{a\ddot{e}}$ for λ=670 nm.

Table 3 shows a summary and comparison of the different forcing terms during Asia-dust episode periods at Gwangju with other sites. Comparing the results obtained for surface aerosol forcing in the visible spectrum, aerosols present during the Asia dust episode at Gwangju had a slight higher tendency to perturb the radiative environment than those reported e.g. for INDOEX and ACE-Asia Gosan. This result however differ from the work reported by Bush et al. (2006), that indicates that the aerosol radiative forcing during ACE-

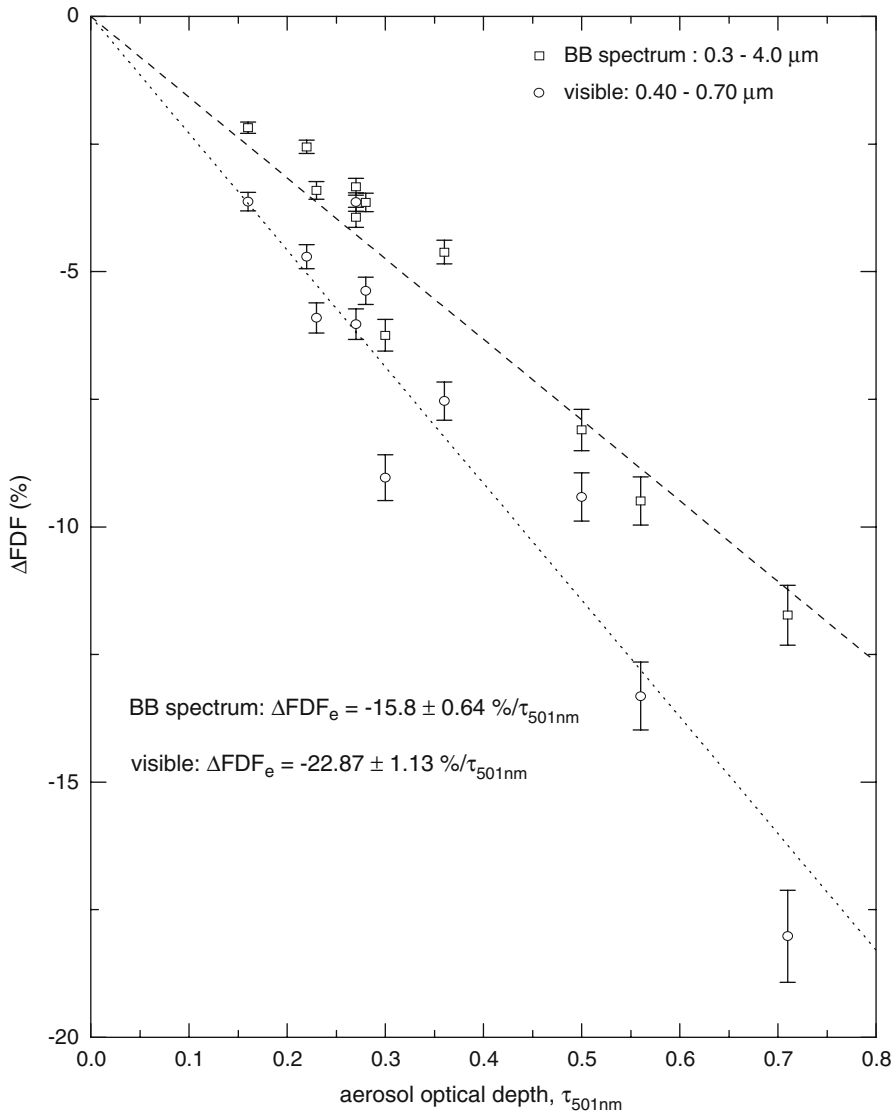

Fig. 6 Broadband and visible band passes fractional diurnal forcing plotted against average daily AOD (λ?λ=501 nm) during the spring time Asian dust episodes of 2000 and 2001. The standard error of the fractional diurnal forcing is represented by the *vertical bar* over each measure of the individual optical depths

Asia campaign in Gosan is smaller in magnitude than that reported for INDOEX and the Tropospheric Aerosol Radiative Forcing Observational Experiment TARFOX (Hignett et al. 1999). This may be explained by the fact that aerosols manifest extremely complex atmospheric profile and types during the dust episodes in North East Asia (Huebert et al. 2003). Thus, larger portions of carbonaceous aerosols may be present in Gwangju during this period than during the INDOEX and Gosan Experiments. This may consequently lead to a greater forcing as expected from abundant absorbing carbonaceous aerosols (Bush et al. 2006).

Conclusion

This study provides some of the first estimates of the surface forcing parameters determined from ground based spectral and radiometric data obtained during the Asia dust spells of 2000 and 2001 at Gwangju, South Korea. Such studies are important for improving aerosol parameterization in radiative transfer models and evaluating regional direct radiative forcing. Daily measurements of AOD at λ=501 nm were computed for every minute between January 2000 and May 2001 during the course of cloud free days. To remove

Table 3 Comparison of the surface forcing efficiency components at Gwangju during the Asia dust episode with some experimental Campaign in North East Asia, Northern Indian Ocean and Europe-Mediterranean

Forcing term	This study	This study	ACE-Asia, Gosan[a]	ACE-Asia, Gosan[a]	INDOEX[b]	INDOEX[b]	Linan, China[c]	Linan, China[c]	Sea of Japan[d]	STAA-ARTE-MED[e]	STAA ARTE-MED[e]
	BB region	Visible region	BB region	visible region	TSR	Visible region	TSR	Visible region	Visible region	Visible region	Total SR
ΔF_e (W m^{-2})	−180.84±6.68	−98.92±4.28	−173.0±32.9	−93.6±12.9	−173.8±30.2	−93.4±12.9	–	−88.7±14.7	–	−60.0±7.3	–
ΔDF_e (W m^{-2})	−81.10±5.14	−47.09±2.20	−73.0±9.6	−42.2±4.8	−72.2±5.5	−42.2±4.8	−78.6±20.6	−38.5±4.0	−44.8±12.7	−57.0±3.9	−64
ΔFDF_e (%)	−15.80±0.64	−22.87±1.13	−18.0±2.3	−26.7±3.3	−16.8±1.2	−26.70±3.3	–	−23.0±2.6	–	–	–

[a] Bush and Valero (2003): March–May 2001; [b] Ramanathan et al. (2001): February–March 1999; [c] Xu et al. (2003): 28 October–1 December 1999; [d] Markowicz et al. (2003): March–April 2001; [e] Formenti et al. (2002): August 1998

cloud contamination, the study employed a cloud-screening filter to reject data points with scatter ratios larger than an empirically determined threshold. Result shows that τ_{501nm} increases from annual average value of 0.34±0.13 to values >0.60 during the major dust event days of April 7–9 2000 and 13 April 2001. The retrieved aerosol optical depths were then used along with the flux measurements to determine the forcing efficiencies. Result shows that as the aerosol optical depth increases, so also the radiative forcing. For example, on the severe dust spell days of 7 April 2000, diurnal average forcing ΔDF was estimated to be −58.4 and −36.6 W m^{-2} and similarly on 25 April 2001, ΔDF was estimated to be −48.2 and −28.6 W m^{-2} for the broadband solar irradiance and visible band pass, respectively. The absolute magnitude of the surface radiative forcing in the broadband and visible spectrum is observed to be highly dependent on the quantity and types of aerosols perturbing the environment. The fractional diurnal forcing efficiencies ΔFDF_e for the broadband and visible spectral region were $-15.8\pm0.64\%/\tau_{501nm}$ and $-22.87\pm1.13\%/\tau_{501nm}$, respectively, indicating that aerosol has a major impact on the environment. Asia dust aerosols are observed to have larger influence on the energy budget of Gwangju during the severe dust spells than other dust free days. Back trajectories analysis of the different air masses approaching Gwangju indicates that the site is being influenced by different source and types of aerosols throughout the measurements periods.

Acknowledgements This work was supported in part by the Korea Science and Engineering Foundation (KOSEF) through the Advanced Environmental Monitoring Research Center (ADEMRC), at Gwangju Institute of Science and Technology. We greatly acknowledge the Alexander von Humboldt (AvH) Foundation and the Meteorological Institute, University of Bonn, for their supports. We are also grateful to the two anonymous reviewers for their thoughtful comments and suggestions, which greatly helped in improving the manuscript.

References

Ackerman, A. S., Toon, O. B., Stevens, D. E., Heymsfield, A. J., Ramanathan, V., & Welton, E. J. (2000). Reduction of tropical cloudiness by soot. *Science, 288*, 1042–1047.

Anderson, G. P., Berk, A., Acharya, P. K., Matthew, M. W., Bernstein, L. S., Chetwynd, J. H., et al. (1999). MODTRAN 4: Radiative transfer modeling for remote sensing.

Optics in Atmospheric Propagation and Adaptive Systems III. In A. Kohnle & J. D. Gonglewski (Eds.), *Proceedings of SPIE, the International Society for Optical Engineering, vol. 3866* (pp. 2–10).

Angstrom, A. (1964). The parameters of atmospheric turbidity. *Tellus, 16*, 64–75.

Beck, A., Anderson, G. P., Acharya, P. K., Chetwynd, J. H., Bernstein, L. S., Shettle, E. P., et al. (1999). MODTRAN4 User's Manual. Hanscom AFB, MA: Air Force Research Laboratory.

Bush, B. C., & Valero, F. P. J. (2002). Spectral aerosol radiative forcing at the surface during the Indian Ocean experiment (INDOEX). *Journal of Geophysical Research, 107*(D19), doi:10.1029/2000JD000020.

Bush, B. C., & Valero, F. P. J. (2003). Surface aerosol radiative forcing at Gosan during the ACE-Asia campaign. *Journal of Geophysical Research, 108*(D23), 8660, doi:10.1029/2002JD003233.

Bush, B. C., Valero, F. P. J., & Pope, S. K. (2006). Atmospheric radiative forcing at the surface derived from aircraft irradiance and spectral optical depth measurements. *Journal of Geophysical Research, 111*, D12207, doi:10.1029/2005JD006321.

Christopher, S. A., Wang, J., Ji, Q., & Tsay, S. C. (2003). Estimation of diurnal shortwave dust aerosol radiative forcing during PRIDE. *Journal of Geophysical Research, 108*, 8596–8607.

Coakley, Jr., J. A., Cess, R. D., & Yurevich, F. B. (1983). The effect of tropospheric aerosols on the earth's radiation budget: A parameterization for climate models. *Journal of Atmospheric Science, 40*, 116–138.

Conant, W. C. (2000). An observational approach for determining aerosol surface radiative forcing: Results from the first field phase of INDOEX. *Journal of Geophysical Research, 105*, 15347–15360.

Dubovik, O., Holben, B. N., Kaufman, Y. J., Yamasoe, M., Smirnov, A., Tanre, D., et al. (1998). Single-scattering albedo of smoke retrieved from the sky radiance and solar transmittance measured from ground. *Journal of Geophysical Research, 103*, 31903–31924.

Dubovik, O., Holben, B. N., Eck, T. F., Smirnov, A., Kaufman, Y. J., King, M.D., et al. (2002). Variability of absorption and optical properties of key aerosol types observed in worldwide locations. *Journal of Atmospheric Science, 59*, 590–608.

Dutton, E. G., Reddy, P., Ryan, S., & DeLuisi, J. J. (1994). Features and effects of aerosol optical depth observed at Mauna Loa, Hawaii: 1982–1992. *Journal of Geophysical Research, 99*, 8295–8306.

Eck, T. F., Holben, B. N., Dubovik, O., Smirnov, A., Goloub, P., Chen, H. B., et al. (2005). Columnar aerosol optical properties at AERONET sites in central eastern Asia and aerosol transport to the tropical mid-Pacific. *Journal of Geophysical Research, 110*, D06202, doi:10.1029/2004JD005274.

Eck, T. F., Holben, B. N., Reid, J. S., Dubovik, O., Smirnov, A., O'Neill, N. T., et al. (1999). Wavelength dependence of the optical depth of biomass burning, urban and desert dust aerosols. *Journal of Geophysical Research 104*, 31333–31350.

Hansell, R. A., Tsay, S., Ji, Q., Liou, K. N., & Ou, S. C. (2003). Surface aerosol radiative forcing derived from collocated ground-based radiometric observations during PRIDE, SAFARI, and ACE-Asia. *Applied Optics, 42*(27), 5533–5544.

Hignett, P., Taylor, J. P., Francis, P. N., & Glew, M. D. (1999). Comparison of observed and modeled direct aerosol forcing during TARFOX. *Journal of Geophysical Research, 104* (D2), 2279–2287.

Holben, B. N., Tanre, D., Smirnov, A., Eck, T. F., Slutsker, I., Abuhassan, N., et al. (2001). An emerging ground-based aerosol climatology: Aerosol optical depth from AERONET. *Journal of Geophysical Research, 106*, 12067–12097.

Huebert, B. J., Bates, T., Russell, P. B., Shi, G., Kim, Y. J., Kawamura, K., et al. (2003). An overview of ACE-Asia: Strategies for quantifying the relationships between Asian aerosols and their climatic impacts. *Journal of Geophysical Research, 108*(D23), 8633, doi:10.1029/2003JD003550.

Intergovernmental Panel on Climate Change (IPCC) (2001). Climate change 2001. In J. T. Houghton, Y. Ding, D. J. Griggs, M. Noguer, P. J. van der Linden, X. Dai, K. Maskell & C. A. Johnson (Eds.), *The scientific Basis* (pp. 881). New York: Cambridge University Press.

Iziomon, M. G., & Lohmann, U. (2003). Characteristics and direct radiative effect of mid-latitude continental aerosols: The ARM case. *Atmospheric Chemistry and Physics, 3*, 1903–1917.

Jacovides, C. P., Kaltsounides, N. A., Asimakopoulos, D. N., & Kaskaoutis, D. G. (2005). Spectral aerosol optical depth and Angstrom parameters in the polluted Athens atmosphere. *Theoretical and Applied Climatology, 81*, 161–167.

Kim, D. H., Sohn, B. J., Nakajima, T., Takamura, T., Takemura, T., Choi, B. C., et al. (2004). Aerosol optical properties over East Asia determined from ground-based sky radiation measurements. *Journal of Geophysical Research, 109*, D02209, doi:10.1029/2003JD003387.

Kim, Y. J., Kim, K. W., & Oh, S. J. (2001). Seasonal characteristics of haze observed by continuous visibility monitoring in the urban atmosphere of Gwangju, Korea. *Environmental Monitoring and Assessment, 70*, 35–46.

King, M. D., Kaufman, Y. J., Tanre, D., & Nakajima, T. (1999). Remote sensing of tropospheric aerosols from space: Past present and future. *Bulletin of America Meteorological Society, 80*, 2229–2259.

Koren, I. Y., Kaufman, Y. J., Remer, L. A., & Martins, J. V. (2004). Measurement of the effect of Amazon smoke on inhibition of cloud formation. *Science, 303*, 1342–1345.

Merrill, J. (2001). ACE-Asia circulation and transport events and patterns. *Eos Trans. AGU, 82*(27), Fall Meet. Suppl., Abstract A22A-0122.

Mitchell, Jr. J., M. (1971). The effect of atmospheric aerosols on climate with special reference to temperature near the Earth's surface. *Journal of Applied Meteorology, 10*, 703–714.

Ogunjobi, K. O., He, Z., Kim, K. W., & Kim, Y. J. (2004). Aerosol optical depth during episodes of Asian dust storms and biomass burning at Gwangju, South Korea. *Atmospheric Environment, 38*, 1313–1323.

Ogunjobi, K. O., Kim, Y. J., & He, Z. (2003). Aerosol optical properties during Asian dust storm episodes in South Korea. *Theoretical and Applied Climatology, 76*, 65–75.

Pinker, R. T., Pandithurai, G., Holben, B. N., Dubovik, O., & Aro, T. O. (2001). A dust outbreak episode in sub-Sahel

West Africa. *Journal of Geophysical Research, 106*(D19), 22923–22930.

Ramanathan, V., et al. (2001). Indian Ocean experiment: An integrated analysis of the climate forcing and effects of the great Indo-Asian haze. *Journal of Geophysical Research, 106*(D22), 28371–28398.

Rosenfeld, D., & Lensky, I. M. (1998). Satellite-based insights into precipitation formation processes in continental and maritime convective clouds. *Bulletin of the America Meteorological Society, 79*, 2457–2476.

Satheesh, S. K., & Ramanathan, V. (2000). Large differences in tropical aerosol forcing at the top of the atmosphere and Earth's surface. *Nature, 405*, 60–63.

Schafer, J. S., Eck, T. F., Holben, B. N., Artaxo, P., Yamasoe, M. A., & Procopio, A. S. (2002). Observed reductions of total solar irradiance by biomass burning aerosols in the Brazilian Amazon and Zambian Savanna. *Geophysical Research Letter, 29*, 1823–1826.

Twomey, S. (1977). The influence of pollution on the shortwave albedo of clouds. *Journal of Atmospheric Science, 34*, 1149–1152.

Won, J., G., Yoon, S., C., Kim, S., W., Jefferson, A., Dutton, E.G., & Holben, B. N. (2004). Estimation of direct radiative forcing of Asian dust aerosols with sun/sky radiometer and lidar measurements at Gosan, Korea. *Journal of the Meteorological Society of Japan, 82*, 115–130.

Xu, J., Bergin, M. H., Greenwald, R., & Russell, P. B. (2003). Direct aerosol radiative forcing in the Yangtze delta region of China: Observation and model estimation. *Journal of Geophysical Research, 108*(D2), 4060, doi:10.1029/2002JD002550.

Yoon, S., C., Won, J., G., Omar, A. H., Kim, S., W., & Sohn, B., J. (2005). Estimation of radiative forcing by key aerosol types in worldwide locations using a column model and AERONET data. *Atmospheric Environment, 39*, 6620–6630.

Yu, H., Kaufman, Y. J., Chin, M., Feingold, G., Remer, L. A., Anderson, T. L., et al. (2005). A review of measurement-based assessment of aerosol direct radiative effect and forcing. *Atmospheric Chemistry and Physics, 5*, 7647–7768.